Calculation of hysteretic force between a superconductor and a magnet

M. J. Qin, G. Li, H. K. Liu, and S. X. Dou
Institute for Superconducting and Electronic Materials, University of Wollongong, Wollongong NSW 2522, Australia

E. H. Brandt
Max-Planck-Institut für Metallforschung, Institut für Physik, D-70506 Stuttgart, Germany

(Dated: February 1, 2008)

The magnetic levitation forces of a superconducting disk (SC) levitated by a cylindrical permanent magnet (PM) have been calculated from first principles for superconductors with finite thickness. The current $j(\rho, z)$ and field $B(\rho, z)$ profiles in the SC in the non-uniform magnetic field generated by the PM have been derived. The levitation force is observed to depend non-linearly on the critical current density j_c and on the thickness of the SC. The flux creep is described by a current-voltage law $E(j) = E_c(j/j_c)^n$, from which we show that the levitation force depends on the speed at which the PM approaches or recedes from the SC, which accounts for the experimentally observed force creep phenomenon. The stiffness of the system has been derived by calculating the minor force loops. The numerical results reproduce many of the features exhibited by experiments.

PACS numbers: 74.60.-w, 74.25.Ha, 74.25.Ld

I. INTRODUCTION

It has been well known that a permanent magnet (PM) can be stably levitated above a high temperature superconductor (HTS) cooled by liquid nitrogen, which has become the well known symbol for HTS technology. This fascinating magnetic levitation results from the interaction of the induced current inside the superconductor with the inhomogeneous magnetic field generated by the PM. Because of its possible industrial applications, such as noncontacted superconducting bearings[1,2], gravimeters[3], flywheel energy storage systems[4,5,6,7,8,9], magnetic levitation transport systems[10], and motors[11], the magnetic levitation between a PM and a HTS has been the subject of intensive studies for the last decade.

The most common feature of the magnetic levitation is the hysteretic behavior of the vertical force F_z versus the distance z between the PM and the HTS when the PM is descending to and then ascending from the HTS. When a PM approaches a zero-field-cooled HTS, the levitation force increases monotonically from zero, as the PM is moving from the HTS, the levitation force decreases sharply to a negative peak at some distance, indicating attractive force between the HTS and the PM, then declines to zero again at larger distance. Detailed experiments have been performed on melt-textured-grown (MTG) YBCO and RBCO (R denotes a rare earth element such as Nd, Sm, Gd, Eu, Dy, Ho, Er, Tm, Yb, Lu and La), thin films, as well as granular samples[4,12,13,14,15]. For MTG YBCO and RBCO samples, the force curve is usually asymmetrical, i.e., the absolute value of the attractive force is smaller than the maximum repulsive force, $|F_{\rm a,max}| < F_{\rm r,max}$. For thin films, the force curve is almost symmetrical $|F_{\rm a,max}| \approx F_{\rm r,max}$[16], while for granular samples, the attractive force is hardly present[17].

Various parameters are very important in determining the levitation force. The most important are the pinning strength (critical current density) of the HTS and the induced shielding current loops inside the HTS. Higher j_c and larger loops are very important to achieve a high levitation force. It has been suggested that the levitation force increases linearly with j_c and more than linearly with the current loops[13]. According to this criterion, the current material of choice for superconducting levitation is MTG YBCO and RBCO samples, because high quality MTG samples with high critical current density and single domain diameters up to 10 cm are currently available by means of melt process[18]. Another reason is its high irreversibility line at liquid nitrogen temperature, which is the normal operating temperature for the magnetic levitation experiments. Although higher critical current density can be achieved in thin films, the levitation force is limited by the thickness of the films.

According to the critical state model[19,20], the levitation force is independent of the speed at which the PM approaches and recedes from the HTS[21]. However, as the thermally activated flux motion is prominent in HTS, resulting in the relaxation of the magnetization (current density),[22] the levitation force which depends on the current density of the HTS is expected to decrease with time (force creep). Experimentally the levitation force is observed to be approximately logarithmic in time and can be well correlated with the thermally activated flux motion in HTS[23].

The thickness of the HTS also drastically influences the levitation force. Because the critical current density is limited, for thin HTS samples, the levitation force increases linearly with the thickness of the HTS. However, beyond a certain thickness, the levitation force is independent of the thickness[24]. Other characteristics of the HTS, such as the anisotropy and the grain orientation inside the MTG samples have been studied and shown to affect the levitation force[14,25]. The stiffness of the PM-

HTS system, which represents the spring constant associated with vibrational motion of the levitation system has been intensively studied. And Experimental results for vertical stiffness, lateral stiffness and cross stiffness have been presented[4,12].

Besides these, the geometry and condition of the PM also affect the levitation force. The size and shape of the PM, the homogeneity and the temperature dependence of the PM magnetization have been shown to influence the levitation force[12].

Although the magnetic levitation between a PM and a HTS can be easily demonstrated and detailed experimental results for the levitation force have been presented, the theoretical models for this magnetic levitation system have not been fully developed yet so far. The first reason is that a model has to consider a finite thickness superconducting disk under a perpendicular magnetic field. In the case of an infinite long cylinder under a parallel applied magnetic field, the magnetic field and current density profiles can be easily obtained by means of the critical state model. However, for a superconducting disk under a perpendicularly applied magnetic field, the extreme demagnetization effects make this case qualitatively different from the parallel field case. The second reason is that the model has to consider the response of a HTS immersed in a non-uniform magnetic field generated by the PM.

In order to avoid the above difficulties, all the models for the magnetic levitation force presented so far have taken different assumptions based on different physical considerations. Most of the models are based on the critical state model[19,20], which has long been used to account for the irreversible properties of type-II superconductors. The image model[26,27,28]treats the superconductor as a pure diamagnet and the PM as a set of magnetic dipoles, if the hysteretic behavior is not important. The system is described by two magnetic dipoles, representing the PM and its mirror image, oppositely magnetized and located the same distance below and above the superconductor surfaces. The advantage of this model is that analytical expressions can be obtained. However it cannot be used to account for the dynamic stiffness. The extension of the image model to include another 'frozen' image of the PM has been introduced to explain the dynamic stiffness of the system[29].

In a recent article by Navau and Sanchez[30], the authors reviewed the model in the critical state. Early model considered only extreme limits such as complete flux exclusion or complete flux penetration, thus described the behavior of type-I superconductors or type-II superconductors with very high critical current[26,31]. This model was later extended to describe the flux penetration[32,33,34]. However, these models assumed a superconducting sample small enough to consider the magnetic-field-gradient constant along it. At the same time, the demagnetization effect due to the finite dimensions of the superconductor has been neglected. Navau and Sanchez[30] have accounted for the demagnetization by introducing a demagnetization factor. However, it should be pointed out that the use of demagnetization factor for superconductors in the mixed state in which current is distributed inside the bulk sample, is qualitatively invalid[35,36]. Although the authors considered a non-uniform field gradient along the sample, the radial magnetic field generated by the PM has been neglected. While in real experiments, the PM is usually smaller than the HTS, in this case the assumption of neglecting the radial field may not be applicable.

The models mentioned above can be used to account for some of the levitation force features exhibited by experiments, however, they are obviously oversimplified. First, the current and field distribution in the HTS under a non-uniform magnetic field have been neglected. For practical applications using the magnetic levitation, the precise control of the interacting force between a superconducting target and the applied non-uniform magnetic field is of critical importance. It is hence necessary to thoroughly understand the hysteretic force characteristics of a superconductor immersed in such fields. From an analytical point of view, a precise knowledge of current and field profiles is essential to the force calculation of the magnetic levitation force between the PM and the HTS. Second, the models are all based on the critical state model, which neglects flux creep effects. However, at the nitrogen temperature, which is the normal operating temperature for the levitation force experiments, the flux creep may play an important role on the levitation force. Numerical analysis such as finite element method (FEM) has been applied to calculate the magnetic levitation force, it is capable of deriving the current and field profiles inside the HTS, but it neglects the flux creep as well.

To better understand the design of the magnetic levitation system between the PM and the HTS, a better model is required. In this paper, taking all the above points into account, we develop a model to describe a more realistic experimental configuration and to account for the experimentally observed features of the magnetic levitation force. The demagnetization effect is considered by calculating the current and magnetization of finite thickness superconductors, and current and field distributions in the superconductor are derived. The flux creep effect is taken into account by using a current-voltage law $E(J) = E_c(J/J_c)^n$.

The paper is structured as follows, In Sec. II we will discuss the theoretical consideration for both the permanent magnet and the superconductor in a non-uniform magnetic field, including assumptions made and numerical considerations. The results of the calculations, including the effects of the HTS geometry and characteristics on the levitation force, the force creep effects, the minor loops and the stiffnesses will be presented and compared with experiments in the literature in Sec. III, and Sec. IV are the concluding remarks.

II. MODELING

A. The Permanent magnet

We consider a superconducting disk with radius a and thickness $2b$, levitated over a co-axial cylindrical permanent magnet with radius R_{PM} and thickness t_{PM}. The top surface center of the PM is taken as the origin of the cylindrical coordinate system (ρ, ϕ, z). Because of the axial symmetry of the system, only the cross section of the system is considered, with the axis direction Z chosen as the symmetry axis of the SC and the PM, and ρ (radial direction) parallel to the surfaces of the SC and the PM. For this configuration, the vector potential of the PM has only one component along the ϕ direction and can be derived by integrating the vector potential of a circular current loop with radius R_{PM} along the thickness t_{PM} as,

$$A_\phi(\rho, z) = \frac{B_{\mathrm{rem}}}{2\pi}\int_0^\pi R_{\mathrm{PM}}\cos\phi \ln\frac{(z+t_{\mathrm{PM}}) + \sqrt{R_{\mathrm{PM}}^2+\rho^2-2\rho R_{\mathrm{PM}}\cos\phi+(z+t_{\mathrm{PM}})^2}}{z+\sqrt{R_{\mathrm{PM}}^2+\rho^2-2\rho R_{\mathrm{PM}}\cos\phi+z^2}}d\phi, \tag{1}$$

where B_{rem} is the remanent induction of the PM. The radial field $B_\rho = -\partial A_\phi/\partial z$ can then be written as,

$$B_\rho(\rho, z) = \frac{B_{\mathrm{rem}}}{\pi}\sqrt{\frac{R_{\mathrm{PM}}}{\rho}}\sum_{i=0}^{1}\frac{(-1)^i}{k_i}\left[\left(1-\frac{1}{2}k_i^2\right)K(k_i) - E(k_i)\right] \tag{2}$$

where K and E are complete elliptic integrals of the first and second kind, respectively. And

$$k_i^2 = \frac{4\rho R_{\mathrm{PM}}}{(R_{\mathrm{PM}}+\rho)^2+(z+it_{\mathrm{PM}})^2}, \qquad i = 0, 1.$$

The field on the axis $B_z = (1/\rho)\partial(\rho A_\phi)/\partial\rho$ is,

$$B_z(\rho, z) = \frac{B_{\mathrm{PM}}}{2\pi}\int_0^\pi \frac{\rho R_{\mathrm{PM}}\cos\phi - R_{\mathrm{PM}}^2\cos^2\phi}{R_{\mathrm{PM}}^2+\rho^2-2\rho R_{\mathrm{PM}}\cos\phi}\sum_{i=0}^{1}\frac{z+it_{\mathrm{PM}}}{\sqrt{R_{\mathrm{PM}}^2+\rho^2-2\rho R_{\mathrm{PM}}\cos\phi+(z+it_{\mathrm{PM}})^2}}d\phi + \frac{A_\phi}{\rho} \tag{3}$$

B. The superconducting disk in a non-uniform magnetic field

The response of superconducting disks and strips in an uniform applied magnetic field has been extensively studied by Brandt[37,38]. We now consider the response of a superconducting disk in the non-uniform magnetic field generated by the PM [Eqs. (2) and (3)]. The calculation is for the zero-field-cooled (ZFC) process, in which the superconducting disk is cooled below its critical temperature T_c in zero applied field and then the non-uniform field is applied to the disk. Screening current is generated inside the superconducting disk. The central idea is to find the equation of motion for the current density. Because of the axial symmetry, the current density J and the vector potential A_J generated by the current have only one component along the ϕ direction. The total vector potential of the system is then $A = A_J + A_\phi$, and the total magnetic field $B = \nabla\times A = \nabla\times A_J$. We assume here the material law $\mathbf{B} = \mu_0\mathbf{H}$, which is a good approximation when the flux density B and the critical sheet current $J_c b$ are larger than the lower critical field B_{c1} everywhere inside the superconducting disk. This requirement is often satisfied in the magnetic levitation measurement, normally operated at a relatively high temperature of 77 K. According to the Maxwell equation with gauge $\nabla\cdot A_J = 0$, we have $\mu_0 J = \nabla\times B = \nabla\times\nabla\times A = \nabla\times\nabla\times A_J = -\nabla^2 A_J$. The solution of this Laplace equation in cylindrical geometry

can be written as

$$A_J(\rho, z) = -\mu_0 \int_0^a d\rho' \int_{-b}^{b} dz' Q(r, r') J(r'), \qquad (4)$$

with $r = (\rho, z)$ and $r' = (\rho', z')$. The integral kernel

$$Q(r, r') = f(\rho, \rho', z - z') + f(\rho, \rho', z + z'), \qquad (5)$$

with

$$f(\rho, \rho', \eta) = \frac{-1}{\pi k}\sqrt{\frac{\rho'}{\rho}}\left[\left(1 - \frac{1}{2}k^2\right)K(k) - E(k)\right] \qquad (6)$$

$$k^2 = \frac{4\rho\rho'}{(\rho + \rho')^2 + \eta^2},$$

K and E are the complete elliptic integrals of the first and second kind, respectively.

Eq. (5) is obtained by integrating the 3D Green function of the Laplace equation, $1/4\pi|r_3 - r_3'|$ with $r_3 = (x, y, z)$, over the angle $\phi = \arctan(y/x)$[38]. The total vector potential can then be written as

$$A(\rho, z) = -\mu_0 \int_0^a d\rho' \int_{-b}^{b} dz' Q(r, r') J(r') + A_\phi(\rho, z) \qquad (7)$$

To obtain the desired equation of motion for the current density $J(\rho, z, t)$, we express the induction law $\nabla \times \mathbf{E} = -\dot{\mathbf{B}} = \nabla \times \dot{\mathbf{A}}$ in the form $\mathbf{E} = -\dot{\mathbf{A}}$. Combining this expression with Eq. (7), we have

$$E(\rho, z) = \mu_0 \int_0^a d\rho' \int_{-b}^{b} dz' Q(r, r') \dot{J}(r') - \dot{A}_\phi(\rho, z) \quad (8)$$

The equation of motion for the current density can be derived by inverting Eq. (8) as

$$\dot{J}(\rho, z) = \frac{1}{\mu_0} \int_0^a d\rho' \int_{-b}^{b} dz' Q^{-1}(r, r')[E(r, r') + \dot{A}_\phi(\rho', z')], \qquad (9)$$

where Q^{-1} is the reciprocal kernel defined by

$$\int_0^a d\rho' \int_{-b}^{b} dz' Q^{-1}(r, r') Q(r', r'') = \delta(r - r'') \qquad (10)$$

It can be seen from Eq. (9) that the equation of motion for the current density contains the reciprocal kernel, which depends only on the geometry of the superconducting sample. Here we consider a disk, but the kernel Q can be changed to calculate other sample geometries, such as strips, and even arbitrary sample shapes[38]. The equation also depends on the applied magnetic field via A_ϕ. Here we consider the field of a permanent magnet given by Eqs. (2) and (3), but one may also use other type of magnetic field, such as the field generated by a circular current loop or by dipoles. Besides these, the equation also depends on the material law $E = E(J)$ of the superconducting sample. Obviously any sufficiently sharply bent $E(J)$ law may be used; in the following we choose the rather general material law $E(J) = E_c(J/J_c)^n$, which yields the limits of the critical state model for $n \to \infty$, the flux flow model for $n = 1$, and the flux creep model for $1 < n < \infty$. Eq. (9) is easily time integrated by starting with $J(\rho, z, t = 0) = 0$ at time $t = 0$ and then putting, $J(\rho, z, t = t + dt) = J(\rho, z, t) + \dot{J}(\rho, z, t)dt$. The vector potential can then be derived from Eq. (7) and the magnetic field is $B = \nabla \times A$. For all the calculations in this paper, we use a reduced unit of $E_c = a = \mu_0 = 1$. And the critical current is assumed to be independent of the magnetic field.

C. The levitation force and the hysteresis loop

The PM approaches and recedes from the HTS as $z = z_0 - z_0 \sin(\omega t) + z_{00}$, where $z_0 + z_{00}$ is the initial distance and z_{00} is the minimum distance between the PM and the HTS, ω represents the speed at which the PM approaches and recedes from the HTS. Experimentally, uncertainty will be caused when the PM touches the HTS, and therefore the limit $z_{00} = 0$ should be avoided. In this calculation we choose $z_{00}/a = 0.1$ as the minimum distance between the PM and the superconducting disk.

As the current density and the magnetic field inside the superconducting disk have been derived, the vertical levitation force along the z-axis can be readily obtained as

$$F_z = 2\pi \int_0^a d\rho \int_{-b}^{b} dz J(\rho, z) B_\rho(\rho, z) \qquad (11)$$

As the applied magnetic field is non-uniform, in order to show the magnetization hysteresis loop, we choose the axis field $B_{\text{axis}} = B_z(\rho = 0, z)$ at the bottom surface center of the superconducting disk to represent the strength of the applied non-uniform field, with

$$B_{\text{axis}} = \frac{B_{\text{rem}}}{2}\left[\frac{z + t_{\text{PM}}}{\sqrt{R_{\text{PM}}^2 + (z + t_{\text{PM}})^2}} - \frac{z}{\sqrt{R_{\text{PM}}^2 + z^2}}\right] \qquad (12)$$

and the magnetic moment

$$m = 2\pi \int_0^a d\rho \int_{-b}^{b} dz \rho^2 J(\rho, z) \qquad (13)$$

D. The minor force loop and the stiffness

Because of the hysteretic behavior of the superconducting disk, when the PM is moved away and back again by

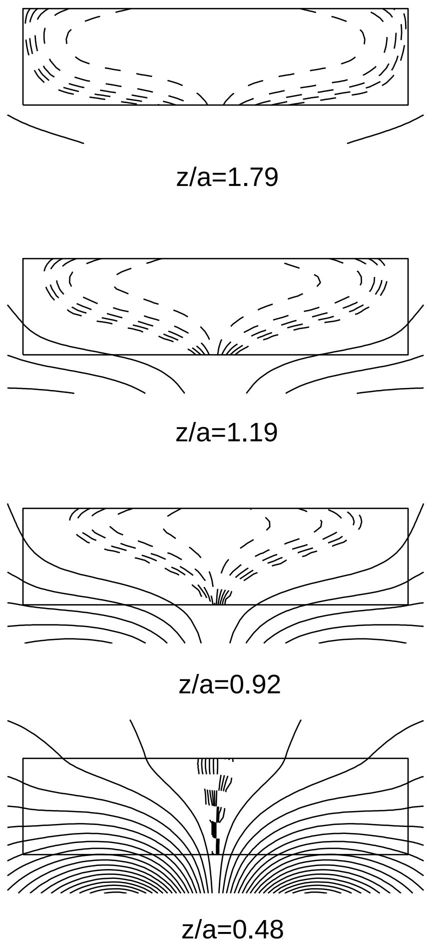

FIG. 1: Magnetic field lines when a PM approaches a superconducting disk with $b/a = 0.25$, $J_c = 1$, and $\sigma = 20$ at distances $z/a = 1.79, 1.19, 0.92, 0.48$. Dashed lines are the contour lines of the current density inside the disk. The PM approaches the disk as $z = z_0 - z_0 \sin(\omega t)$ with a frequency of $\omega = 0.1$.

a small amount δz at a distance z, the $F_z(z)$ curve follows a minor force loop rather than the major force loop. For small δz, the minor force loop is reversible, but beyond a certain δz, hysteretic behavior in the minor force loop will be observed. The stiffness at different distance z can then be derived as $K_z = -\partial F_z/\partial z$.

III. RESULTS AND DISCUSSIONS

A. Current and field profiles in the HTS

The magnetic flux lines when the PM is approaching the superconducting disk with side ratio $b/a = 0.25$ and $\sigma = 20$, $J_c = 1$ are shown in Fig. 1 as solid lines at distances $z/a = 1.79$, 1.19, 0.92 and 0.48. The dashed lines are the contour lines of the current density inside the disk. Fig. 1 shows the penetration of the non-uniform magnetic field generated by the PM into the superconducting disk. Some features different from those of the superconducting disk in uniform magnetic field[37] can be clearly seen. Because the magnetic field is stronger at the bottom of the disk (see $z/a = 0.48$ of Fig. 1), the penetration starts from the bottom of the disk, while the top surface is not penetrated. The resulting magnetic field fronts inside the disk form an onion-shape rather than the symmetrical lens-shape observed for homogeneous applied field.

Fig. 2 shows the profiles of the current density $J(x, y)$ corresponding to Fig. 1. The current density first saturates at the edges of the bottom surface, while the current density at the edges of the top surface is smaller ($z/a = 1.79$). As the PM is moving closer, the saturation spreads both into the top surface and into the middle of the disk ($z/a = 1.19$ and $z/a = 0.92$), until it is saturated everywhere inside the disk ($z/a = 0.48$). Because we choose $\sigma = 20$, the maximum current density is much smaller than the critical current density $J_c = 1$. Increasing σ will result in a larger current density close to J_c.

The magnetic field lines when the PM is moving away from the superconducting disk with side ratio $b/a = 0.25$ and $\sigma = 20$, $J_c = 1$ are shown in Fig. 3 as solid lines at distances $z/a = 0.12$, 0.20, 0.32 and 0.48. The dashed lines are the contour lines of the current density inside the disk. And Fig. 4 shows the corresponding profiles of the current density $J(x, y)$. As the magnetic field is decreased, the current density is reversed inside the disk. What is interesting is that the reversion begins at the bottom surface with $x/a = \pm 0.5$, where the magnetic field is strongest. As the PM is moving away further, the reversion spreads onto the top surface and middle of the disk (Fig. 4, $z/a = 0.20$ and $z/a = 0.32$), until the current is completely reversed ($z/a > 0.48$). Note that for a superconducting disk immersed in a uniform magnetic field, the reversion usually begins at the edge of the disk and spreads into the center of the sample. As the levitation force is determined by the current density $J(x, y)$ and the magnetic field shown in Fig. 1 to Fig.4, the features shown in these figures will be reflected in the levitation force as will be discussed in the following.

The magnetic field lines and the profiles of the current density $J(x, y)$ depend on the side ration b/a, σ and critical current density J_c of the superconducting disk, as well as the dimensions of the PM. Detailed results will be presented elsewhere.

B. Geometry of the HTS on F_z

As we use reduced units of $E_c = a = \mu_0 = 1$ in this calculation, the effect of the HTS geometry on the levitation is demonstrated by calculating the levitation force for different thicknesses $2b$ of the superconducting disk. The results are shown in Fig. 5a, where $F_z(z)$ curves at $\sigma = 2$, $\omega = 0.1$ and $J_c = 1$ for different thicknesses $2b$ are plotted. The F_z curves show typical hysteretic behavior. For larger side ratio b/a, the hysteretic loop is

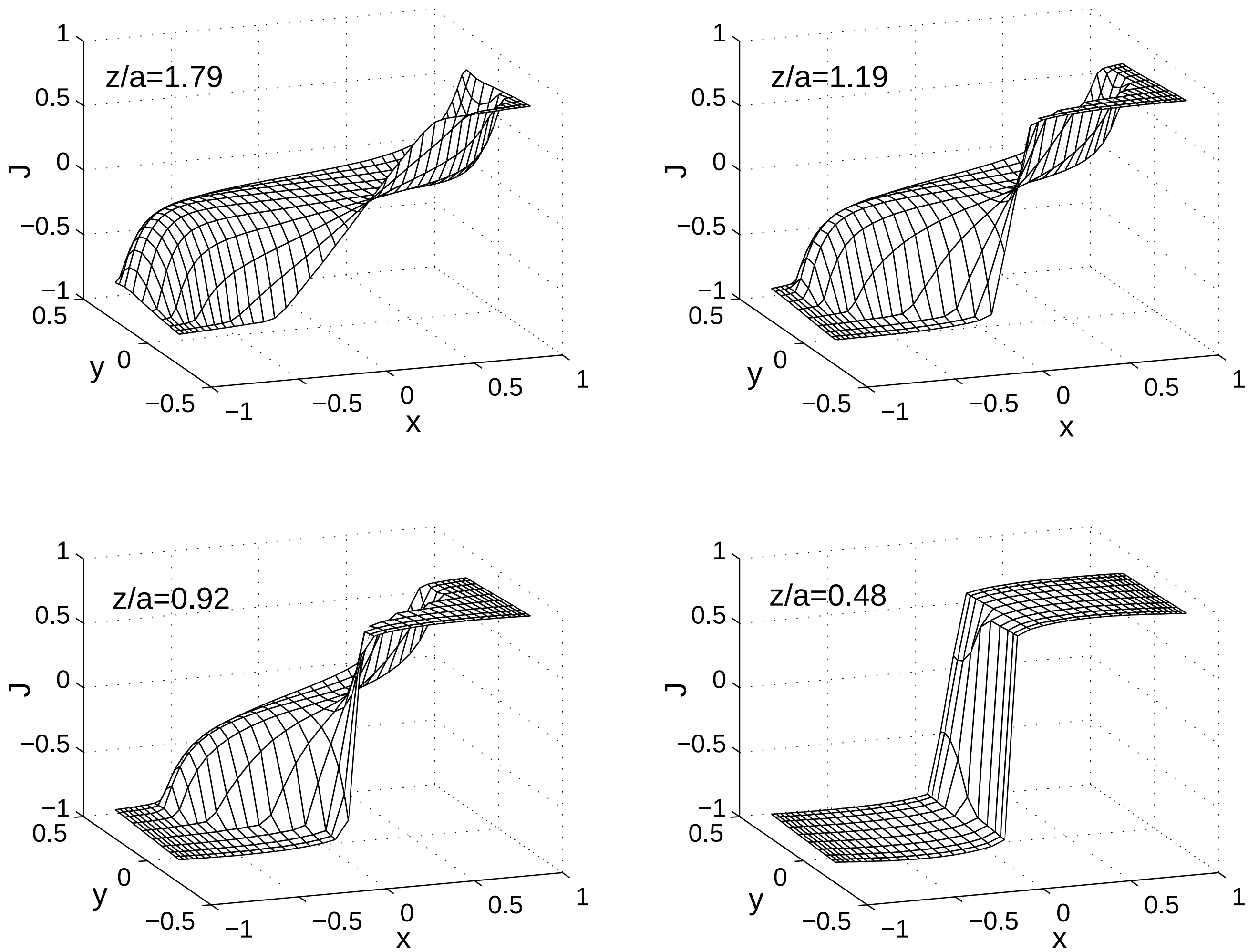

FIG. 2: Current profiles $J(x, y)$ for the same disk as in Fig. 1.

asymmetrical, with the maximum repulsive force larger than the maximum attractive force. However, as the side ratio is decreased, the hysteretic force loop becomes more and more symmetrical. For $b/a = 0.05$, the curve is completely symmetrical. Experimentally, symmetrical F_z versus z curves have been observed in YBCO thin film[16], while in MTG bulk samples, F_z versus z curves are usually asymmetrical. The reason for this is easy to understand: For a thin sample, the magnetic moment is saturated when the PM is close to the sample. When the PM is moving away from the sample, only a little decrease in the applied field saturates the magnetic moment in the reverse direction, results in a symmetrical magnetization hysteresis loop (see Fig. 5b, where the magnetization hysteresis loops corresponding to Fig. 5a are plotted), and therefore a symmetrical force loop. While for a bulk sample the magnetic moment saturates when the PM is close to the sample, it is never saturated in the reverse direction when the PM is moving far away from the disk (see the magnetization hysteresis loops for $b/a \geq 0.8$ in Fig. 5b), resulting in an asymmetric hysteresis loop of the magnetization and therefore an asymmetric loop of the force versus distance.

Another interesting feature shown in Fig. 5 is that a maximum is found in the repulsive force when the PM is at some distance away from the HTS, rather than at the minimum distance. Experimentally this maximum has been observed in thin films[16], while it was hardly observed in MTG samples. Riise et al. accredited this maximum to the dimensions of the PM, which tends to vanish with larger $t_{\rm PM}$ and smaller $R_{\rm PM}$. And the disappearance of the maximum in MTG sample was explained noting that bulk samples are less sensitive to a non-uniform field than films[16]. Another explanation comes from Sanchez and Navau[32], who claimed that this maximum is a result of the minimum in the derivative of the field produced by the PM, based on a constant-field-gradient model[30]. They concluded that the maximum depends crucially on

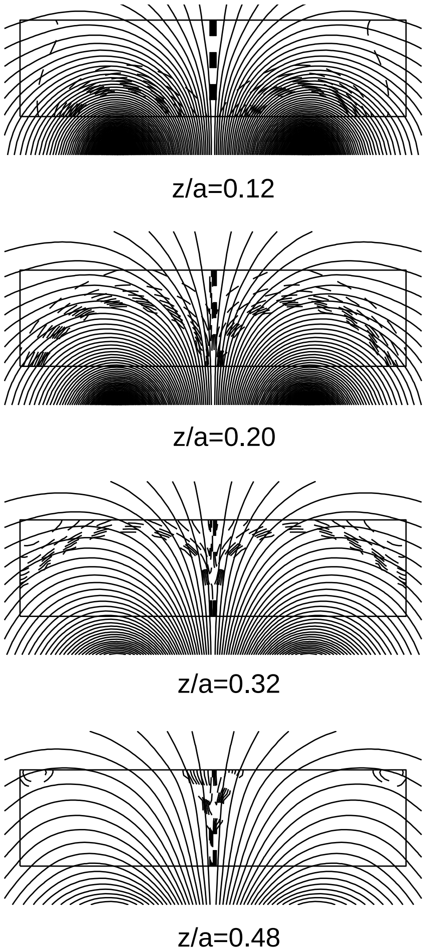

FIG. 3: Magnetic field lines when a PM is moving away from a superconducting disk with $b/a = 0.25$, $J_c = 1$, and $\sigma = 20$ at distances $z/a = 0.12, 0.20, 0.32, 0.48$. Dashed lines are the contour lines of the current density inside the disk. The PM recedes from the disk as $z = z_0 - z_0 \sin(\omega t)$ with a frequency of $\omega = 0.1$.

the side ratio b/a, the larger the side ratio b/a, the closer the maximum shifts to zero PM-HTS separation. When b/a is sufficiently large, the maximum may not exist. However, as can be seen from Fig. 5a, the maximum is independent of the side ratio b/a. The peaks are observed to be at the same distance for all side ratios and even for $b \gg a$ not shown here. In a separate calculation, we have found that this maximum is independent of the dimensions of the PM. We conclude that the peak arises from the intrinsic properties of the HTS. As will be seen from figures below, the maximum depends on the creep exponent σ. The larger σ, the closer the maximum shifts to zero PM-HTS separation. When σ is sufficiently large, the maximum may not be observed any more.

Because $\sigma = n - 1$, and n can be related to the pinning potential of the sample as $n = U_0(T, B)/k_B T$[37,38], smaller σ means lower pinning potential or higher temperature. Both MTG YBCO and YBCO thin film have a relatively high pinning potential, however experimentally when a PM approaches a thin film, it may increase the local temperature on the film, resulting in a lower σ, and therefore in the maximum. On the other hand, although the PM may increase the temperature of the surface of the bulk sample, the currents flow in a much larger volume and the levitation force is determined by the bulk properties, therefore the maximum may not be observed in MTG bulk samples.

In the inset of Fig. 5a, we show the maximum repulsive force as a function of the side ratio b/a. It can be seen from the figure that for small side ratio b/a, the maximum repulsive force increases linearly with b/a, but saturates as b/a is further increased. Technically, a superconducting disk with diameter $2a$ approximately equal to the thickness may be optimum for magnetic levitation, further increase of the thickness will not enhance the levitation force. This calculated result is consistent with the experimental observations[24].

C. Characteristics of the HTS on $\mathbf{F}_\mathrm{z}$

Characteristics of the HTS in this calculation are represented by two parameters. One is the creep exponent σ related to the pinning potential by $n = \sigma + 1 = U_0(T, H)/k_B T$; another one is the critical current density J_c representing the pinning strength. The effect of σ on the magnetic levitation force is shown in Fig. 6a, where the vertical magnetic levitation force F_z versus the distance z at $b/a = 1.4$, $\omega = 0.1$ and $J_c = 1$ for different pinning potentials of the superconducting disk are plotted. It can be seen from Fig. 6a that as σ is increased, the hysteretic force loop increases and the maximum repulsive force shifts to smaller PM-HTS separation. When σ is sufficiently large, the peak is not observed, as discussed in the above section (the maximum at $\sigma = 100$ corresponds to minimum HM-HTS separation). On the contrary, the maximum in the attractive force shifts to larger PM-HTS separation with increasing σ. The maximum attractive force increases with σ, however, when σ is larger than 5, it decreases again and saturates at higher σ. As opposed to this, the maximum repulsive force increases monotonically with σ and reaches a saturation value at large σ, as shown in the inset of Fig. 6a.

Fig. 6b shows the corresponding magnetization hysteresis loops. For $\sigma = 1$, the pinning potential is very small, because of the relaxation effects, the applied magnetic field can penetrate deeper into the sample, similar to the case of small side ratio b/a shown in Fig. 5. The magnetization hysteresis loop and therefore the force loop are symmetric. Increasing the pinning potential (larger σ) results in larger hysteresis loops of the magnetization. However, further increase of σ leads to a reversible response and to a smaller magnetization hysteresis loop. Interestingly, the peak in the maximum attractive force corresponds to the maximum hysteresis of the magnetization (here $\sigma = 5$) as can be seen from Fig. 6, which is also the case in Fig. 5.

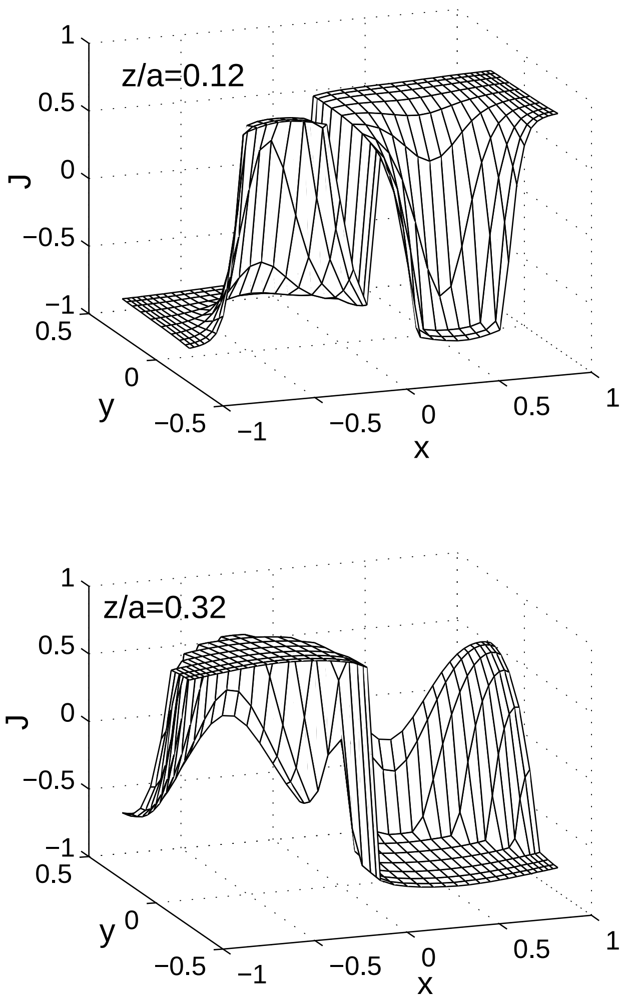

FIG. 4: Current profiles $J(x, y)$ for the same disk as in Fig. 3.

The sharp decrease of the levitation force from repulsive to attractive results from the non-uniform magnetic field generated by the PM and from the relaxation of the current in the HTS. According to Eq. (11), the vertical levitation force is determined by the radial magnetic field for the PM and the current density of the HTS. The radial magnetic field is strongest close to $x/a = \pm R_{\rm PM}$ at the bottom of the disk [see Eq. (2)]. Therefore, the radial magnetic field and the current close to $x/a = \pm R_{\rm PM}$ on the bottom of the disk contribute more to the levitation force. When the applied field is decreased by a small amount, the current close to $x/a = \pm R_{\rm PM}$ on the bottom of the disk is reversed to positive first, although the total current is still negative (the magnetic moment is negative), the levitation force decreases sharply to a negative value, because the attractive force results from the current close to $x/a = \pm R_{\rm PM}$ at the bottom of the disk is much larger than the repulsive force resulting from the negative current in the HTS. For a small σ, because of relaxation, the current is small, and only a small decrease in the applied magnetic field may lead to a complete reversal of the current, see Fig. 6, therefore the maximum attractive force is closer to zero PM-HTS separation. When σ is increased, the current is larger, more decrease of the applied magnetic field is needed to reverse the current. Therefore the maximum attractive force is larger and shifts to larger PM-HTS separation. Further increasing σ shifts the maximum attractive force to larger PM-HTS separation, but the maximum attractive force is smaller. This is because much more decrease of the applied magnetic field is needed to reverse the larger current when σ is increased, although the current is larger but the radial field is smaller, resulting in a smaller maximum attractive force observed in Fig. 6a.

Another characteristics of the HTS which drastically influences the magnetic levitation force is the critical current density of the HTS. The calculated results of $F_{\rm z}$ versus z curves at $b/a = 1.4$, $\sigma = 20$ and $\omega = 0.1$ for different

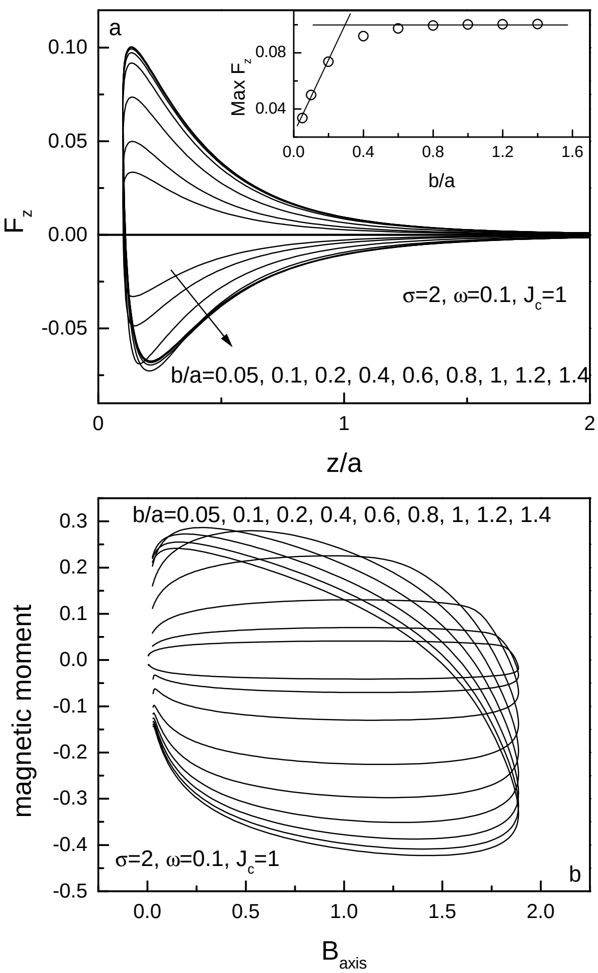

FIG. 5: (a) The vertical magnetic levitation force F_{z} versus the distance z at $\sigma = 2$, $\omega = 0.1$ and $J_c = 1$ for different thicknesses of the superconducting disk. Inset shows the maximum repulsive force as a function of the thickness, solid lines are guide for the eyes only. (b) The corresponding magnetization hysteresis loops.

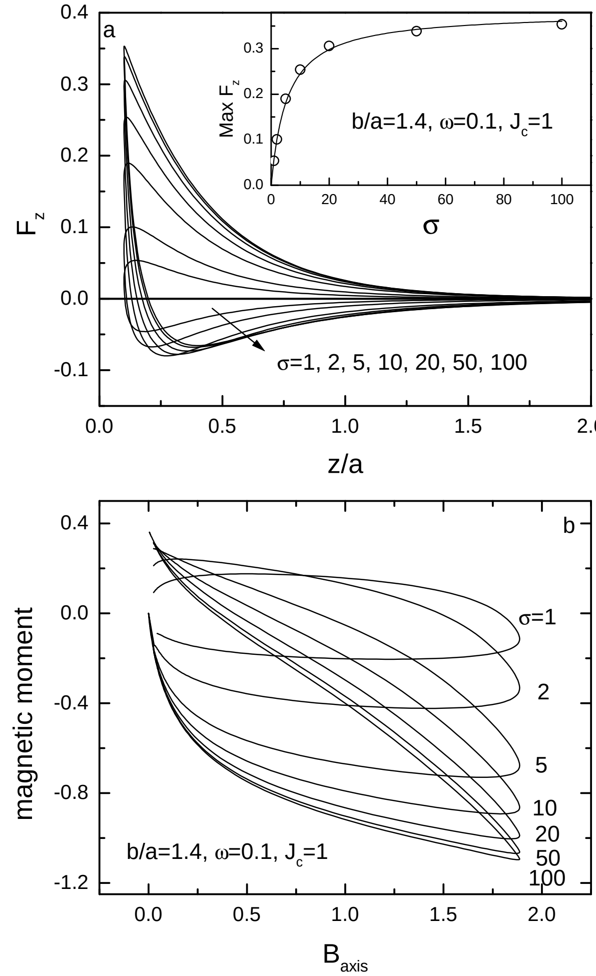

FIG. 6: (a) The vertical magnetic levitation force F_{z} versus the distance z at $b/a = 1.4$, $\omega = 0.1$ and $J_c = 1$ for different pinning potentials of the superconducting disk. Inset shows the maximum repulsive force as a function of σ, the solid line is a guide for the eyes only. (b) The corresponding magnetization hysteresis loops.

critical current densities J_c are plotted in Fig. 7a. The corresponding magnetization hysteresis loops are shown in Fig. 7b. For small critical current densities ($J_c \leq 10$), the calculated results are typical F_{z} versus z curves, which show both the repulsive force branch and the attractive force branch. The attractive force branches of the curves are hidden by the large vertical axis scale. However, when J_c is larger than 20, no attractive force is observed. When J_c is larger than 60, the F_{z} versus z curves are almost reversible ($\sigma = 80, 100$). This result can also be seen from the magnetization hysteresis loops, as shown in Fig. 7b. Increasing the critical current density leads to larger hysteresis loop and then to reversible magnetization hysteresis loops. Experimentally, F_{z} versus z curves with very small hysteresis width has been observed in a MTG sample[12], indicating a very high critical current density in this sample.

Based on the critical state model, the constant-field-gradient model[32] predicted that the maximum repulsive force depends linearly on the critical current density. In order to study this dependence, we plot in the inset of Fig. 7a the dependence of the maximum repulsive force as a function of the critical current density shown as open circles. It is obvious that the dependence is a nonlinear function. The linear dependence is observed only at very low critical current density $J_c < 5$. A fitting to the obtained data results in the dependence

$$F_z = \frac{3.3 J_c}{9.3 + J_c}, \tag{14}$$

shown as solid line in the inset. From Eq. (14) we can see that the maximum repulsive force saturates at high critical current density.

Experimentally it is very difficult to get systematic results as shown in Fig. 6 and Fig. 7, however, Fig. 6 and Fig. 7 can be used as a quick reference for testing the

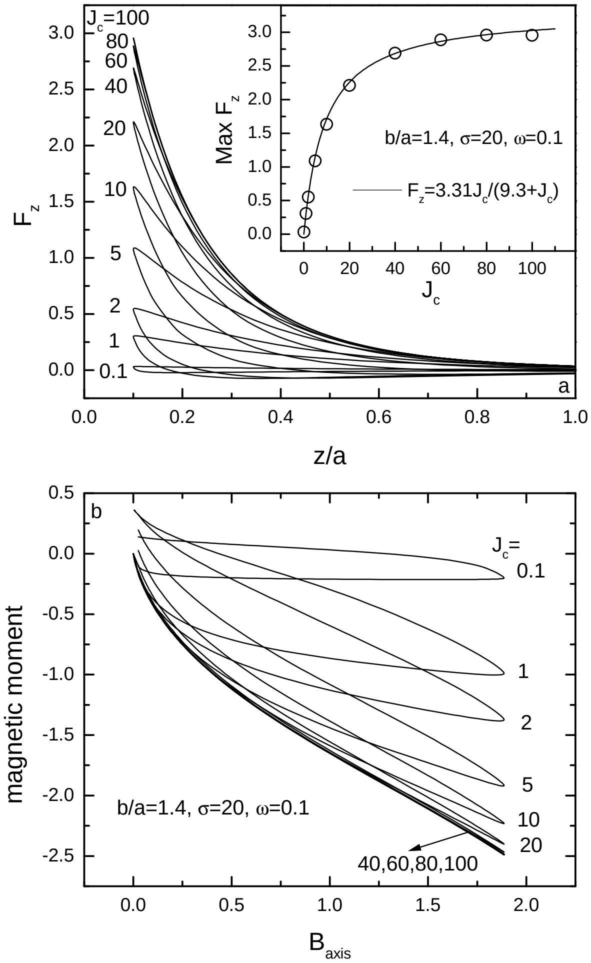

FIG. 7: (a)The vertical magnetic levitation force F_z versus the distance z at $b/a = 1.4$, $\sigma = 20$ and $\omega = 0.1$ for different critical current densities of the superconducting disk. Inset shows the maximum repulsive force as a function of J_c, the solid line is a fit with $F_z = 3.31 J_c/(9.3 + J_c)$. (b)The corresponding magnetization hysteresis loops.

properties of the sample under investigation. By comparing the experimental results with Fig. 6 and Fig. 7, one may have an idea about the pinning potential and critical current of the sample.

D. Force creep

It has been well known that the current density in HTS experiences relaxation (decay with time), which has been extensively studied both theoretically and experimentally in terms of the magnetization. Because the vertical magnetic levitation force is determined by the current density in the HTS and radial magnetic field generated by the PM, it is expected that the levitation force may exhibit relaxation, resulting in a time dependent levitation force in experiments. However, reports on this dynamic behavior are very few[23,39]. On the other hand, no models so far have taken this relaxation behavior of the magnetic levitation force into account. This is quite surprising considering the operating temperature of the levitation system between a HTS and a PM, which is normally at the relatively high temperature of 77K, where the relaxation rate is usually quite high. It is also surprising if one considers the effects of the force decay on the design of any practical applications invoking PM-HTS levitation.

In this calculation, the force relaxation is taken into account by using a voltage-current law $E(J) = E_c(J/J_c)^n$. With $1 < n < \infty$, this material law describes the flux creep in terms of the magnetization inside the superconducting disk. In Fig. 8 we show the F_z versus z curves at $b/a = 1.4$, $\sigma = 2$ and $J_c = 1$ for different frequencies ω at which the PM approaches and recedes from the HTS. It is obvious that the levitation force depends on the speed at which the PM approaches and recedes from the HTS; larger speed leads to a larger force loop. On the contrary, previous models based on the critical state model assume that the levitation force is independent of the speed at which the PM approaches and recedes from the HTS[12].

In the inset of Fig. 8a, we show the maximum repulsive force as a function of the time $t = 1/\omega$ as open circles in a double logarithmic plot. The linear dependence is obvious. Fitting to the data gives a $F_z \propto t^{-m}$ dependence of F_z on time. This result actually arises from the thermally activated flux motion in the HTS, because the voltage current law $E(J) = E_c(J/J_c)^n$ is actually a result of the current dependence of the activation energy $U(J) = U_0 \log(J_c/J)$; this can be shown by using the Arrhenius law $E = Bv = Bv_0 \exp[-U(J)/k_BT]$. With this activation energy, the relaxation of the current density can be derived as $J \propto t^{-m}$, leading to the force relaxation shown in the inset of Fig. 8a. Experimentally, the force creep has been observed to be logarithmic in time[23] within a narrow time window. It is expected that a non-logarithmic force creep will be observed if an extended time window is measured.

The force relaxation can also be clearly seen from Fig. 8b, where the magnetization hysteresis loops corresponding to Fig. 8a are plotted. The magnetization hysteresis loops increase with increasing frequency. This behavior is similar to the so-called dynamic magnetic moment relaxation measurement, in which the DC magnetization hysteresis loops are measured at different sweep rates of the applied magnetic moment. The magnetization hysteresis loop increases with increasing sweep rate. It has been proven that the dynamic magnetic moment relaxation is equivalent to the normal relaxation measurement, in which the magnetic moment is recorded as a function of time at fixed temperature and magnetic field, when studying the relaxation of HTS[40,41]. Therefore, by measuring the vertical levitation force F_z versus z at different frequencies with which the PM approaches and recedes away from the HTS, one can study the relaxation of the force as well as the current density of the HTS.

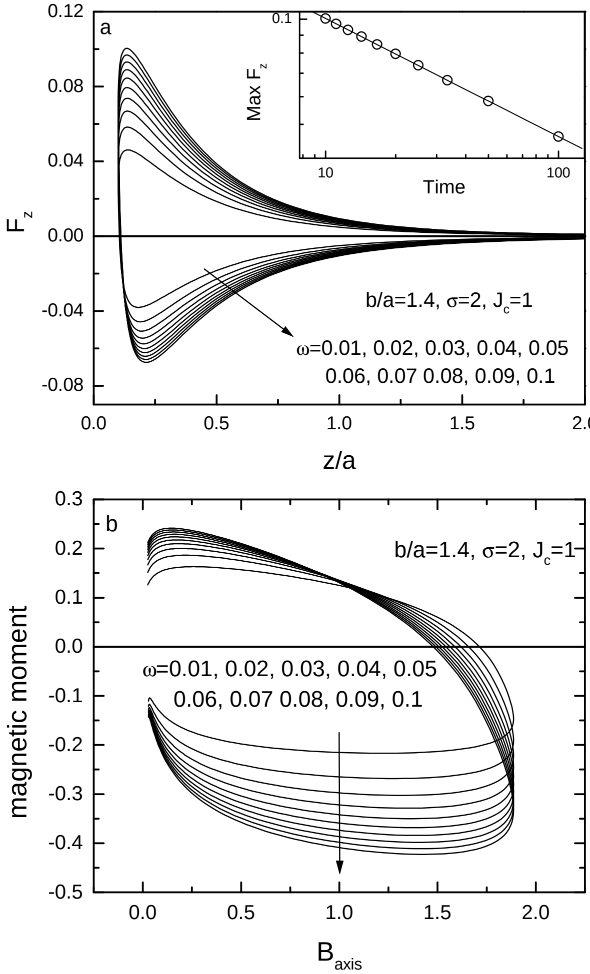

FIG. 8: (a)The vertical magnetic levitation force F_{z} versus the distance z at $b/a = 1.4$, $\sigma = 2$ and $J_c = 1$ for different frequencies at which the PM approaches and recedes from the HTS. Inset shows the relaxation of the levitation force. (b)The corresponding magnetization hysteresis loops.

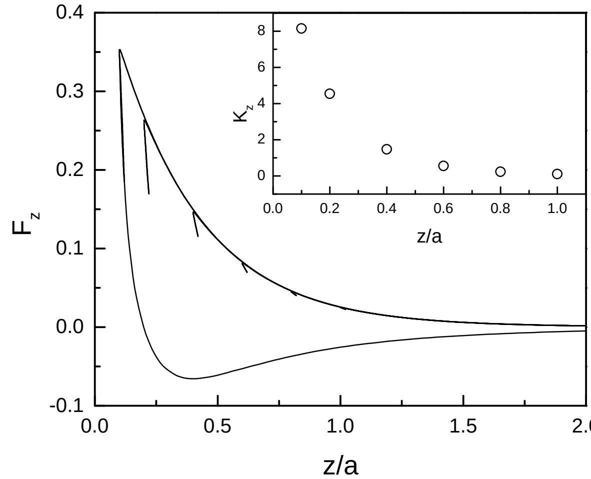

FIG. 9: (a)The vertical magnetic levitation force F_{z} versus the distance z at $b/a = 1.4$, $\sigma = 100$, $\omega = 0.1$ and $J_c = 1$. The minor force loops at different distances z are shown with a amplitude $\delta z = 0.02a$. Inset shows the stiffness of the system.

E. Minor force loops and stiffness

One of the most important parameters used to characterize the magnetic levitation system using a PM and a HTS, is the magnetic stiffness defined as $K_{\mathrm{z}} = -\partial F_{\mathrm{z}}/\partial z$, which represents the spring constant associated with vibrational motion of a levitation system. The magnetic stiffness can be determined by measuring or computing minor force loops. The calculated minor force loops at different PM-HTS separations for $b/a = 1.4$, $\sigma = 100$, $\omega = 0.1$ and $J_c = 1$ are shown in Fig. 9. Here we use an amplitude of $\delta z = 0.02a$, resulting in reversible minor force loops. Higher amplitude will lead to hysteretic behavior not shown here. The calculated vertical stiffness is plotted in the inset as a function of the PM-HTS distance z. It can be seen from Fig. 9 that $K_{\mathrm{z}} > 0$, indicating a stable levitation between a PM and a HTS. K_{z} decreases with increasing PM-HTS separation z. K_{z} may also depend on other parameters, such as J_c, ω, σ and the shapes of both the PM and the HTS. All these cases are easily computed by our numerical method. Detailed results will be presented elsewhere.

IV. CONCLUSIONS

The current density and magnetic field profiles of a superconducting disk (SC) with radius a and thickness $2b$ immersed in the non-uniform magnetic field generated by a permanent magnet (PM) are calculated from first principles for the superconductor. From the derived current density, the magnetic levitation force between the SC and the PM has been derived by assuming a voltage-current law $E(J) = E_c(J/J_c)^n$ and a material law $\mathbf{B} = \mu_0\mathbf{H}$. The geometry and characteristics of the SC drastically influence the vertical levitation force F_{z}. F_{z} depends non-linearly on the critical current density j_c of the SC: $F_z = 3.31J_c/(9.3+J_c)$. For thin samples, F_{z} depends linearly on the thickness of the sample, but beyond a certain thickness, F_{z} is mostly independent of the thickness. The flux creep also plays an important role on the magnetic levitation force, which is observed to be non-logarithmic in time. The stiffness for the SC and PM system has also been derived. The calculated results reproduce many of the features for the magnetic levitation between a SC and a PM exhibited by experiments.

V. ACKNOWLEDGMENT

The authors would like to thank the Australian Research Council for financial support.

[1] J. R. Hull, E. F. Hilton, T. M. Mulcahy, Z. J. Yang, A. Lockwood, and M. Strasik, J. Appl. Phys. **78**, 6833 (1995).
[2] B. R. Weinberger, L. Lynds, J. R. Hull, and U. Balachandran, Appl. Phys. Lett. **59**, 1132 (1991).
[3] J. M. Goodkind, Rev. Sci. Instrum. **70**, 4131 (1999).
[4] J. T. Hull, Supercond. Sci. Technol. **13**, R1 (2000).
[5] J. R. Hull, K. L. U. T. M. Mulcahy, R. A. Erick, and R. G. Abboud, Appl. Supercond. **2**, 449 (1994).
[6] H. Kameno, Y. Miyagawa, R. Takahata, and H. Ueyama, Appl. Supercond. **9**, 992 (1999).
[7] H. J. Bornemann, T. Ritter, C. Urban, O. Zaitsev, K. Weber, and H. Rietschel, IEEE. Trans. Appl. Supercond. **2**, 439 (1994).
[8] Q. Y. Chen, Z. Xia, K. B. Ma, C. K. McMichael, M. Lamb, R. S. Cooley, P. C. Fowler, and W. K. Chu, Appl. Supercond. **9**, 457 (1994).
[9] T. A. Coombs, A. M. Campbell, I. Ganney, W. Lo, T. Twardowski, and B. Dawson, Mater. Sci. Eng. B **53**, 225 (1998).
[10] M. Tosa and A. K. Yosihara, in *Fourth International symposium on Magnetic Suspension Technology* (Hampton, VA, NASA, 1998), p. 179.
[11] B. Oswald, M. Krone, M. Soll, T. Stresser, J. Oswald, K. J. Best, W. Gawalak, and L. Kovalev, IEEE. Trans. Appl. Supercond. **9**, 1201 (1999).
[12] J. R. Hull and A. Cansiz, J. Appl. Phys. **86**, 6396 (1999).
[13] M. Ullrich, A. Leenders, and H. C. Freyhardt, Appl. Phys. Lett. **68**, 2735 (1996).
[14] D. Shi, D. Qu, S. Sagar, and K. Lahiri, Appl. Phys. Lett. **70**, 3606 (1997).
[15] W. Hennig, D. Parks, R. Weinstein, and R. P. Sawh, Appl. Phys. Lett. **72**, 3059 (1998).
[16] A. B. Riise, T. H. Johansen, H. Bratsberg, M. R. Koblischka, and Y. Q. Shen, Phys. Rev. B **60**, 9855 (1999).
[17] P. Z. Chang, F. C. Moon, J. R. Hull, and T. M. Mulcahy, J. Appl. Phys. **67**, 4358 (1990).
[18] M. Murakami, *Melt Processed High-Temperature Superconductors* (World Scientific, Singapore, 1992).
[19] C. P. Bean, Phys. Rev. Lett. **8**, 250 (1962).
[20] C. P. Bean, Rev. Mod. Phys. **36**, 31 (1964).
[21] F. C. Moon, *Superconducting Levitation* (Wiley, New York, 1994).
[22] Y. Yeshurun and M. P. Malozemoff, Phys. Rev. Lett. **60**, 2202 (1988).
[23] A. B. Riise, T. H. Johansen, H. Bratsberg, and Z. J. Yang, Appl. Phy. Lett. **60**, 2294 (1992).
[24] J. Unsworth, J. Du, B. J. Crosby, and J. C. Macfarlane, IEEE. Trans. Magn. **29**, 108 (1993).
[25] B. A. Tent, D. Qu, D. Shi, W. J. Bresser, P. Boolchand, and Z. Z. Cai, Phys. Rev. B **58**, 11761 (1998).
[26] Z. J. Yang, J. Supercond. **5**, 529 (1992).
[27] Z. J. Yang, Appl. Supercond. **2**, 559 (1994).
[28] Z. J. Yang and J. R. Hull, J. Appl. Phys. **79**, 3318 (1996).
[29] A. A. Kordyuk, J. Appl. Phys. **83**, 610 (1998).
[30] C. Navau and A. Sanchez, Phys. Rev. B **58**, 963 (1998).
[31] F. Hellman, E. M. Gyorgy, D. W. J. Jr., H. M. O'Bryan, and R. C. Sherwood, J. Appl. Phys. **63**, 447 (1988).
[32] A. Sanchez and C. Navau, Physica C **268**, 46 (1996).
[33] T. Torng and Q. Y. Chen, J. Appl. Phys. **73**, 1198 (1992).
[34] P. Schönhuber and F. C. Moon, Appl. Supercond. **2**, 253 (1994).
[35] M. Däumling and D. C. Larbalestier, Phys. Rev. B **40**, 9350 (1989).
[36] L. W. Conner and A. P. Malozemoff, Phys. Rev. B **43**, 402 (1991).
[37] E. H. Brandt, Phys. Rev. B **58**, 6506 (1998).
[38] E. H. Brandt, Phys. Rev. B **54**, 4246 (1996).
[39] F. C. Moon, P. Z. Chang, H. Hojaji, A. Barkatt, and A. N. Thorpe, Japan. J. Appl. Phys. **29**, 1257 (1990).
[40] H. G. Schnack, R. Griessen, J. G. Lensink, C. J. van der Beek, and P. H. Kes, Physica C **197**, 337 (1992).
[41] M. Jirsa, L. Pust, H. G. Schnack, and R. Griessen, Physica C **207**, 85 (1993).